SERS of cells: What can we learn from cell lysates?

E. Genova [a], M. Pelin [b], G. Decorti [c, e], G. Stocco [b], V. Sergo [d], A. Ventura [c, e], A. Bonifacio [d, *]

[a] PhD School of Reproduction and Developmental Sciences, University of Trieste, 34127 Trieste, Italy
[b] Dept. of Life Sciences, University of Trieste, 34127 Trieste, Italy
[c] Dept. of Medicine, Surgery and Health Sciences, University of Trieste, 34127 Trieste, Italy
[d] Dept. of Engineering and Architecture, University of Trieste, 34127 Trieste, Italy
[e] Institute for Maternal and Child Health IRCCS Burlo Garofolo, Via dell'Istria 65/1, Trieste, 34137, Italy

HIGHLIGHTS

- A rapid and label-free SERS method to analyze cellular environment is proposed.
- A directly probe of cytosol without nanoparticles internalization into cells is presented.
- The method allows to obtain repeatable SERS spectra of cell lysates.

GRAPHICAL ABSTRACT

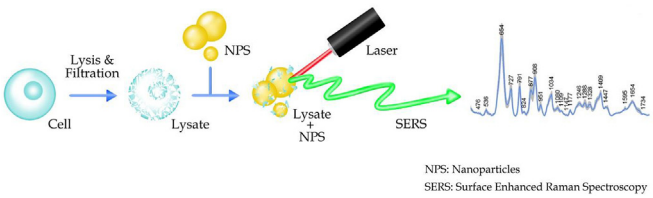

ARTICLE INFO

Accepted 10 December 2017

Keywords:
SERS
Raman
Nanoparticles
Silver
Gold
Cell lysates

ABSTRACT

Surface-enhanced Raman spectroscopy (SERS) is a promising and emerging technique to analyze the cellular environment. We developed an alternative, rapid and label-free SERS-based method to get information about the cellular environment by analyzing cells lysates, thus avoiding the need to incorporate nanoparticles into cells. Upon sonicating and filtrating cells, we obtained lysates which, mixed with Au or Ag nanoparticles, yield stable and repeatable SERS spectra, whose overall profile depends on the metal used as substrate, but not on the buffer used for the lysis process. Bands appearing in these spectra were shown to arise mostly from the cytosol and were assigned to adenine, guanine, adenosine and reduced glutathione (GSH). Spectral differences among various cell types also demonstrated that this approach is suitable for cell type identification.

1. Introduction

The scientific community has paid close attention to the many biomedical applications of nanostructures over the past two decades. In particular, the topic "nano-bio interface", i.e. how nanomaterials interact with biological systems, has raised a strong interest [1–4]. The aim of the studies found in the literature is to clarify the physicochemical interactions at the nano-bio interface but also to exploit them for new biomedical applications. For instance, nanomaterials can be used as innovative cellular [3,5,6] and biochemical sensors with therapeutic potential [6,7]. In particular, gold and silver nanoparticles, which are widely studied and used in many applications of nanotechnology, are interesting systems to study interactions involved at the nano-bio interface [8–10]. Currently, there are several analytical techniques, involving the use of nanoparticles, suitable to characterize the nano-bio interface [2,8,11–13]. Among these techniques, surface-enhanced Raman spectroscopy (SERS) is a vibrational spectroscopy applied to this aim. The SERS effect induces a huge enhancement (with factors varying between 10^6-10^{11}) of the vibrational spectroscopic

* Corresponding author.
E-mail address: abonifacio@units.it (A. Bonifacio).

signal of molecules adsorbed on nanostructured metal surfaces, including metal nanoparticles [14–17].

SERS has been often applied to the analysis of intact eukaryotic cells, using metal nanoparticles as nano-probes to analyze the biochemical composition of cellular environments [18–20]. This approach requires the internalization of nanoparticles into cells, which can be achieved in different ways: by delivery by physical or mechanical methods (e.g. microinjection), by passive diffusion, or by active uptake (endocytosis) [21–23]. Uptake by endocytosis, following the incubation with nanoparticles directly added to the culture medium, is the most commonly used internalization strategy. However, in this way nanoparticles are trapped inside vesicles (i.e. endosomes) and thus they do not enter in the cytosol. Functionalization of the nanoparticle surface, for instance with peptides [22], is usually needed to allow their release into the cytosol or to target specific subcellular structures. However, the functionalized nanoparticle surface can hardly act as a probe for the cellular environment, so that these nanoparticles are usually employed for drug delivery or photo-thermal therapy, rather than for sensing.

One possible alternative to study cells with SERS could be the analysis of cellular lysates instead of intact cells. Using lysates, spectral information about specific subcellular structures is lost. On the other hand, cellular environments such as the cytosol, otherwise inaccessible to nanoparticles up-taken by endocytosis, becomes readily accessible for analysis. Very recently, Hassoun et al. [24] published a paper using SERS spectra of cell lysates, obtained using Ag nanoparticles, to classify tumor cells. The aim of this work is to further explore the application of SERS to cell lysates, investigating and characterizing lysates spectra obtained from both Ag and Au nanoparticles, as a mean to study cellular environment. In particular, a direct measurement and characterization of cytosol composition, otherwise impossible with conventional approaches, was carried out through SERS spectra of cell lysates.

2. Materials and methods

2.1. Cell culture

The immortalized human hepatic IHH cell line was obtained through stable transfection with recombinant plasmid SV40. The primary culture was isolated by surgery from the healthy liver of a male patient affected by intestinal neoplasia [25]. The cell line was maintained in Dulbecco's modified Eagle's medium (DMEM) high glucose with the addition of 10% fetal bovine serum (FBS), 1.25% L-glutamine 200 mM, 1% penicillin 10000 I.U./mL, streptomycin 10 mg/mL, 1% HEPES buffer 1 M, 0.01% human insulin 10^{-4} M and 0.04% dexamethasone 1 mg/mL. The hepatic tumor human HepG2 cell line was maintained in Minimum Essential Medium Eagle (EMEM) with the addition of 10% FBS, 1% L-glutamine 200 mM, 1% penicillin 10000 I.U./mL, streptomycin 10 mg/mL and 1% Na-pyruvate 100 mM. The human cervix carcinoma Hela cells were maintained in DMEM high glucose with the addition of 10% FBS, 1% L-glutamine 200 mM, 1% penicillin 10000 I.U./mL, streptomycin 10 mg/mL. Cell cultures were maintained according to standard procedures in a humidified incubator at 37 °C and with 5% CO_2 and cell passage was performed once a week. All chemicals were purchased from Sigma-Aldrich and used as received.

2.2. Lysate processing

Cell lysate samples were prepared by lysing 5×10^6 IHH, HepG2 or HeLa cells at room temperature with three different types of lysis buffer: i) sodium citrate at the concentration of 10 mM pH 4.4, ii) RIPA buffer pH 7.4 (prepared by mixing Tris-HCl 1 M pH 7.4, NP-40 1%, sodium − deoxycholate 0.5%, SDS 0.1%, NaCl 5 M, EDTA 0.5 M, NaF 50 mM in distilled water) and iii) Lysis buffer pH 7.4 (prepared mixing Tris-HCl pH 7.4 10 mM, EDTA 100 mM, NaCl 100 mM, SDS 0.1% in distilled water). The resulting lysates were successively filtered (Amicon Ultra 3 K Centrifugal filter devices, cut off 10 kDa) by centrifugation at 14000*g*, 4 °C for 30 min. All samples were stored at −80 °C until SERS analysis.

2.3. Cellular fractions preparation

The fractionation process was done for IHH cells in order to separate four different cellular compartments and to analyze them separately with SERS spectroscopy. The cellular fractions of nuclei, cell organelles (lysosome, peroxisome, and mitochondria), membranes and cytosol were obtained centrifuging cell lysates (3×10^7 IHH cells in 2.5 mL of sodium citrate) at different speeds. Briefly, to separate nuclei, the lysate was initially centrifuged at 600 g for 10 min, then the supernatant was recovered and centrifuged at 5000 g for 5 min to obtain a pellet containing lysosome, peroxisome, and mitochondria. Finally, the supernatant was recovered for the last time and ultra-centrifuged (using *Beckman optima* L *Miotti* with rotor type 50 Ti) at 83000 g for 1 h at 4 °C to obtain a pellet that contains membranes, and the supernatant which consists of the cytosolic fraction. All samples were stored at −80 °C until SERS analysis.

2.4. Cell cycle synchronization

IHH cells were exposed to synchronization through *serum starvation* technique, with arrest in G_0/G_1 cell cycle phase [26].

Briefly, two 25 cm^2 flasks, with cells growing at 30–40% of confluence, were washed twice with 5 mL of D-phosphate-buffered saline (D-PBS) and, successively, culture medium lacking fetal bovine serum was added. The flasks were incubated for 72 h. After this time of incubation, cells from one flask were collected, while the other one was re-stimulated adding 7 mL of complete medium culture; this flask was recovered after re-stimulation with complete medium culture for 48 h. Cells were then collected, washed with 5 mL of D-PBS in order to eliminate culture medium residues, counted and finally lysed. The efficiency of cell cycle synchronization was verified by flow cytofluorimetric DNA content analysis, that allows the determination of cells percentage distribution in the three cell cycle phases [27].

2.5. SERS substrate preparation and characterization

Gold and silver nanoparticles were respectively synthesized by Turkevich [28] and Lee-Meisel [29] methods. Briefly, to synthesize gold nanoparticles, 10.6 mg of $HAuCl_4$ were dissolved in 25 mL milliQ-water, then the solution was heated rapidly with vigorous stirring. When the solution started boiling, 750 μL of aqueous citrate trisodium solution (1 wt %) were added drop by drop. The mixture was boiled for 20 minutes after the citrate addition. To synthesize silver nanoparticles, 22.5 mg of $AgNO_3$ were dissolved in 125 mL milliQ-water. The solution was heated with constant stirring. After boiling, 2.5 mL of aqueous citrate trisodium solution (1% wt/v) were rapidly added. The mixture was further boiled for one hour. For the preparation of both Ag and Au nanoparticles, all glassware was carefully cleaned with concentrated solutions of strong acids (aqua regia for Au, HNO_3 for Ag), and then carefully rinsed with milliQ-water. Both gold and silver colloids were stored in the dark at room temperature. SERS substrates were characterized by UV–visible absorption spectroscopy to verify repeatability using a Lambda 20bio UV–vis spectrometer (Perkin-Elmer, Monza, Italy). Both Au and Ag colloids presented some batch-to-batch

variability in size-distribution, as indicated by the three extinction spectra shown in Fig. S1 as Supplementary Information, which are representative of three different size-distributions. The maximum of extinction band occurred, on average, at 537 nm for Au and at 408 nm for Ag. These values are consistent with the literature [28,30]. TEM images of the colloidal Au and Ag nanoparticles are also shown as Supplementary Information (Figs. S2 and S3).

2.6. SERS instrumentation

SERS spectra were collected using an inVia Raman microscope (Renishaw plc, Wotton-under-Edge, UK) in the range of 400–1800 cm^{-1}. The instrument is equipped with 785 nm NIR diode laser (Toptica Photonics AG, Germany) delivering 120 mW of power at the sample. The spectrograph with a 1800 l/mm grating yielded a spectral resolution of 4 cm^{-1}. A × 10 microscope objective (numerical aperture 0.25) was used for data acquisition. Calibration of spectrograph was done with the lines of a Neon lamp, and the calibration was checked prior to each measurement using the 520 cm^{-1} band of a silicon reference sample. Data were acquired using the software WiRE 3.4 (Renishaw).

2.7. Sample preparation for SERS measurements

All types of samples (non-synchronized cell lysates, synchronized cell lysates and cellular fractions) were prepared for the SERS analysis using the same method. Samples were mixed using a micropipette with Au or Ag colloidal nanoparticles in a 1.5 mL polypropylene tube, with a 1:4 lysate-substrate ratio for a final volume of 25 μL (i.e. 5 + 20 μL). The samples were first transferred onto a UV-vacuum quality CaF_2 microscope slide and then placed under the Raman microscope to start the spectra acquisition. We used CaF_2 slides to avoid the typical interference due to fluorescence, which is characteristic of standard glass microscope slides. SERS spectra were then acquired focusing the laser at the top of the drop with an exposure time of 10 s.

2.8. Data preprocessing, analysis and visualization

All SERS data processing was performed within the R software environment for statistical computing and graphics [31]. In particular, for graphical representation of this set of data the *hyperSpec* package was used [32]. Preprocessing consisted in the subtraction of baseline and normalization. The complete preprocessing consisted of three steps: (i) baseline correction, (ii) smoothing interpolation to project the spectra on an evenly spaced wavenumber axis (using the function spc.loess from package *hyperSpec*), and (iii) intensity vector normalization. For the baseline correction, a polynomial baseline (4th order) was fit automatically to the whole spectral range and was subtracted from each spectrum of the dataset, using the function modpolyfit from package *baseline* [33].

Cell cycle data were analyzed by a two way-ANOVA followed by Bonferroni's post test (Prism GraphPad, version 6.0) and statistical significance considered for $p < .05$.

3. Results and discussion

Intense SERS spectra are obtained from lysates only after filtration with a cutoff at 10 kDa, whereas addition of nanoparticles to unfiltered lysates yield weak spectra (Fig. 1). The reason for this lies in the formation of a protein corona on the surface of metal nanoparticles [34,35] exposed to protein solutions, which interferes with the formation of nanoparticle aggregates, necessary for generating a strong SERS effect. The formation of protein

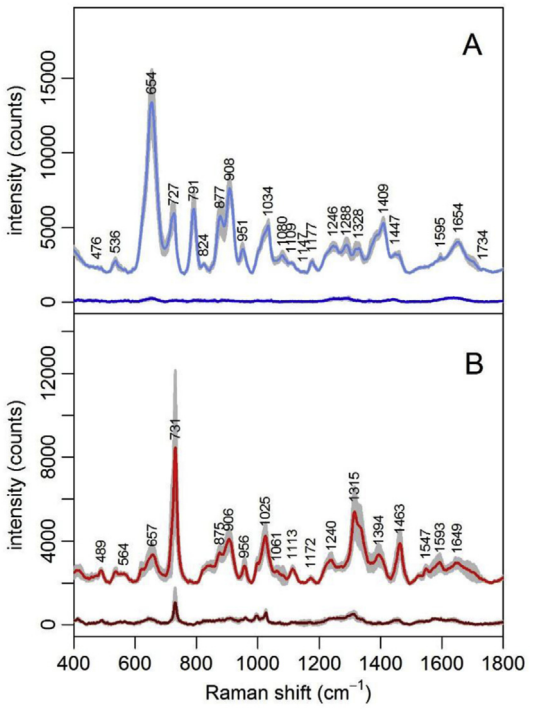

Fig. 1. Effect of filtration. Average SERS spectra of 11 lysates of IHH cells using (A) Ag and (B) Au nanoparticles as substrates. In both (A) and (B), spectra are slightly stacked for better clarity: top spectra (light blue and light red) are from filtered lysates (10 kDa cutoff), bottom spectra (dark blue and dark red) are from unfiltered lysates. Average spectra are obtained from 4 independent measurements out of 2 different cell cultures. Beside each average spectrum, intensity standard deviation (±1 SD) is shown in shaded grey. (For interpretation of the references to color in this figure legend, the reader is referred to the Web version of this article.)

coronas can thus be avoided by de-proteinizing the sample, leading to a stronger SERS effect. In fact, in SERS intense signal amplification occurs mostly at the gap between nanoparticles, also called "hot spots", which in colloidal systems are formed upon partial nanoparticle aggregation. A similar situation, in which SERS intensity dramatically increased upon de-proteinization, has been also observed in the case of colloid-based SERS of blood serum and plasma [36,37]. We have also tried de-proteinization with other methods (i.e. by adding $HClO_4$ 6N) with similar results (Fig. S4 in Supplementary Information). However, filtration is better since it does not require the addition of reagents, which could interfere with the analysis by changing the chemical composition as well as the pH of the samples. The average final protein concentration after filtration was quantified with UV–Vis spectroscopy (see Table S1 in Supplementary Information). An alternative approach consists in the pre-aggregation of metal colloids before their addition to the lysates. Using this method, Hassoun et al. [24] obtained SERS spectra from lysates using Ag nanoparticles which are similar to ours, with small differences possibly due to the different Ag colloid preparation protocol. Interestingly, the same lysate sample gives a different SERS spectrum depending on the metal used as a substrate, in spite of the fact that both Au and Ag nanoparticles are prepared using citrate, and are both coated with negatively-charged citrate molecules. This is another example on how crucial the nature of the metal substrate is in modulating the interaction with the sample.

Spectra similar to those in Fig. 1A were also reported by other authors investigating live, intact cells [38] using electroporation to deliver the Ag nanoparticles inside nasopharyngeal carcinoma cells (C666), human squamous carcinoma cells (A431) and human

Burkitt's lymphoma cells (CA46), as well as in different cancerous renal cells (ACHN, A498 and HEK 293), fixed by drying before addition of Ag nanoparticles [39]. This similarity between SERS spectral profiles (i.e. the relative intensity patterns) of filtered lysates and intact cells suggests that the lysis process and the deproteinization step do not heavily alter the biochemical composition of the sample as detected by SERS. On the other hand, SERS spectra of nanoparticles uptaken by endocytosis are rather different [21], corroborating the hypothesis that filtered lysates yield spectra which are closer to those given by biomolecules found in the cytosol of intact cells than those due to species found in endosomes. This is consistent with the fact that, during filtration, nuclei, organelles (which remain intact after lysis) and membranes are eliminated from the lysate sample. We also noted that, while SERS spectra collected from nanoparticles up-taken by endocytosis are rather heterogeneous and present different spectra, depending on nanoparticles incubation time [21], spectra collected from lysates are repeatable (as shown by the intensity standard deviation in Fig. 1) and do not present any time dependence. These differences can be explained by the fact that filtered lysates are homogeneous samples, while endosomes present a greater heterogeneity, also leading to a higher variability in nanoparticle aggregation kinetics.

The assignment of most intense bands of SERS of lysates (Fig. 2) was done through the comparison of single SERS spectra of nucleobases (adenine, guanine, cytosine, uracil), nucleosides (adenosine, guanosine), nucleotides (adenosine mono- and triphosphate, guanosine triphosphate, nicotinamide adenine dinucleotide, inosine monophosphate) and other biomolecules (e.g. glutathione), all shown in the Figs. S5–S10 as Supplementary Information. We have found that characteristic bands present in the SERS spectra of lysates can be attributed to vibrational modes of adenine, guanine, adenosine [40–42] and reduced form of glutathione (GSH), all of which are present in the cytosol fraction. In particular, SERS spectra of lysates obtained on Ag nanoparticles are dominated by bands given by GSH, with a minor contribution of adenine, whereas those obtained on Au nanoparticles are dominated by bands given by adenine and adenosine, with minor contributions of guanine and GSH.

The type of molecules appearing in these SERS spectra, i.e. nitrogen-containing heterocyclic aromatic species (like purines) and thiols, are those which are known to usually strongly interact with Ag and Au substrates, yielding intense SERS spectra. Purines were observed to dominate SERS spectra of other biofluids such as serum, plasma and tears [36,43,44]. Nucleotide forms of nucleobases, however, were not found to yield SERS spectra with the substrate used (i.e. citrate-reduced Ag and Au nanoparticles). This was not surprising, since phosphate backbones are negatively charged and are thus subject to a repulsive force with the citrate layer coating the metal nanoparticles, hindering their interaction [45,46].

Differences between SERS spectra of lysates obtained from different cell lines were then evaluated. We have analyzed one human hepatic cell line (IHH), one human hepatic carcinoma cell line (HepG2) and one human cervical carcinoma cell line (HeLa) with Ag and Au colloidal nanoparticles as SERS substrate. SERS spectra of lysates are rather similar between different cell lines, when the same metal substrate is used (Fig. 3). Indeed, SERS spectra of different cell lines acquired with Ag substrates are almost identical, while those acquired with Au nanoparticles present some differences. However, these differences are limited to relative band

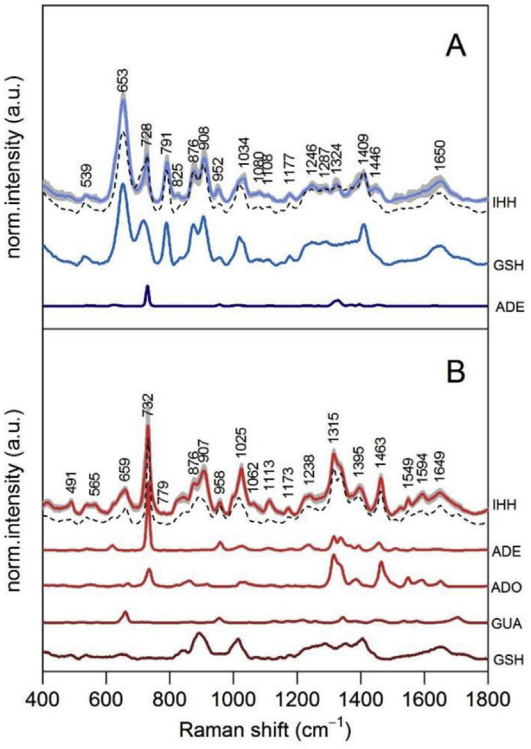

Fig. 2. Comparison between average SERS spectrum of 11 IHH lysates (IHH) on Ag (A) and Au (B) nanoparticles, and corresponding SERS spectra of some biomolecules which were found to be major spectral components, weighted by their contribution to the IHH lysate spectrum: adenine (ADE), adenosine (ADO), guanine (GUA) and glutathione (GSH). Dashed lines represent the "fitted" spectrum, i.e. the spectral sum of all components as displayed in this figure.

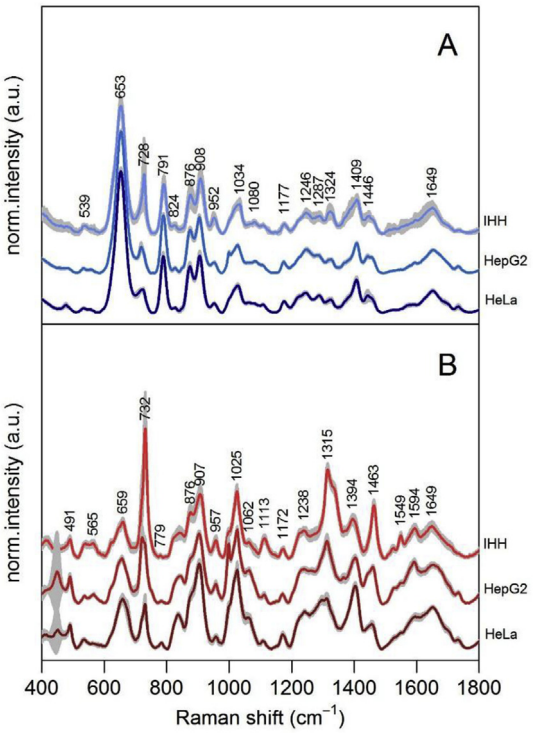

Fig. 3. Comparison between average normalized SERS spectra of filtered lysates from different cells lines (i.e. IHH, HepG2 and HeLa) with silver (A) and gold (B) substrates. For all lysates, the same lysis buffer, i.e. sodium citrate, was used. Each average spectrum is obtained from N independent measurements (N = 24 for IHH and 12 for other cell lines) out of several (2–4) different non-synchronous cell culture flasks, containing cells of the same cell-line and grown using the same method. Beside each average spectrum, intensity standard deviation (±1 SD) is shown in shaded grey.

intensity and do not affect the overall spectral profile. In other words, Au substrates appear to be more sensitive to the cell-line used, with some cell-lines lysates (i.e. IHH) being richer in adenine and adenosine but poorer in GSH with respect to other lines. It should be stressed that these spectral differences cannot be due to different cell phases, since each spectrum in Fig. 3 was averaged from lysates obtained from different non-synchronous cell culture flasks, containing cells of the same cell-line and grown using the same method. Thus, the differences observed must represent real differences between different lines.

These spectral differences could be principally due to the different basal concentrations of deoxynucleosidestriphosphate (dNTPs), nucleosidestriphosphate (NTPs) and adenosine in normal and tumor cells [47–49]. Tumor cells such as HepG2 and HeLa have higher concentrations of adenosine, dNTPs and NTPs respect to normal cells such as IHH. In particular, in tumor cells the concentration of dNTPs and NTPs are respectively 6–11 and 1.2–5 times larger than that of normal cells [47–49]. Since adenine has a much more intense band at 732 cm^{-1} than adenosine, and species with phosphate moieties are not detected because of their electrostatic repulsion with the metal nanoparticles, cells which converted adenine to adenosine, dNTPs and NTPs are thus expected to show a weaker signal around 730 cm^{-1}, as indeed observed in Fig. 3. In other words, in tumor cell lines a lower concentration of the free base adenine, as observed in SERS spectra, could be due to higher relative concentrations of adenosine, dNTPs and NTPs. These differences between different cells lines suggest that SERS of lysates could be used as a rapid and inexpensive identification method for different kinds of cells (i.e. tumor vs non-tumor cells). The fact that these differences are greater for spectra on Au substrates than those on Ag substrates, or, in other words, that Au substrates are more sensitive toward differences between different cell-lines, is due to the fact that adenine bands have a greater relative intensity on Au substrates than on Ag substrates. Ag substrates, on the other hand, favor the adsorption of GSH, whose concentration, as detected by SERS, apparently does not show a significant variation among the cell-lines studied. These observations are in agreement with what reported in a recent work [24], in which SERS spectra of lysates were used to build a predictive model for tumor cell classification, with excellent sensitivity, specificity and accuracy.

To assess to which extent the lysis method might affect SERS spectra, and if spectra obtained from lysates using different methods can be compared, variations between spectra generated by lysates prepared with different lysis buffers were investigated. In particular, cell lysates prepared with sodium citrate 10 mM, RIPA buffer, and lysis buffer were analyzed with SERS. The selection of RIPA buffer and lysis buffer was due to their extensive use in scientific protocols [50–53], whereas sodium citrate was chosen because citrate is already present as adsorbate on the nanoparticles (SERS spectra of sodium citrate are shown in Fig. S11 as Supplementary Information). Moreover, sodium citrate is the buffer most frequently used for quantification of certain drugs (for instance, thiopurine metabolites) in cells by means of high-performance liquid chromatography-mass spectrometry (HPLC-MS) [54]. Fig. 4 displays a comparison between these three different lysis methods, showing that, in most cases, the method used has little impact on SERS spectra. Minor differences (mostly concerning the relative intensity of bands) are observed between SERS spectra of lysates from different lysis buffers, while the main spectral structure is maintained. In particular, RIPA buffer and lysis buffer do not affect SERS spectra with gold nanoparticles substrate. However, RIPA buffer affects SERS spectra when Ag substrates are used, sometimes causing the appearance of a broad, intense band at 1562 cm^{-1}. At the moment, we do not have an explanation for this variability, and must consider it in general as the result of a complex

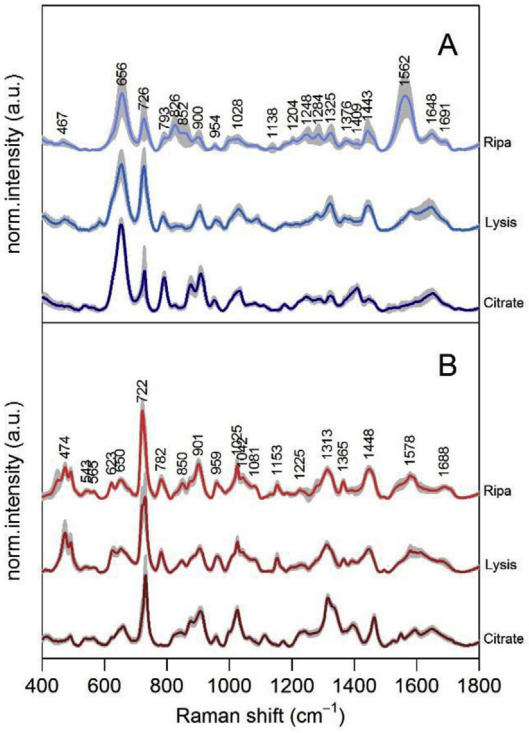

Fig. 4. Comparison between average normalized SERS spectra of filtered lysates from IHH cells obtained with different lysis buffers (i.e. RIPA, Lysis and Citrate buffers), with silver (A) and gold (B) substrates. Average spectra are obtained from N independent measurements (N = 13, 12 and 24 for the RIPA, Lysis and Citrate buffers, respectively) out of at least 3 different cell cultures. Beside each average spectrum, intensity standard deviation (±1 SD) is shown in shaded grey.

interplay between the buffer components, the lysate constituents and the Ag substrate. With the exception of the samples obtained from the RIPA buffer, it can be concluded from these data that our method to study cellular environment of human cells can be applied to different lysis protocols, with minimal variations in the spectra.

Focusing on SERS spectra of lysed IHH, we then aimed at corroborating our hypothesis that SERS spectra are due to species found in the cytosol. The cytosolic fraction of the lysate was separated from other fractions (i.e. membranes, nuclei and organelles) by centrifugation, and was analyzed by SERS after filtration (Fig. 5), together with the other fractions for comparison. Based on the close match between the spectra of the cytosolic fraction and those of the un-fractioned lysate (Fig. 5), it can be concluded that most bands in SERS spectra of filtered lysates are indeed due to the cytosolic components. This is consistent with the fact that the lysate spectra are similar to those obtained from live intact cells [38,39]. On the other hand, membranes and organelles, like nuclei, are mostly intact after lysis and centrifugation process, and are thus almost completely eliminated from the sample after filtration [55]. Membranes, organelles and nuclei fractions yielded SERS spectra nonetheless (Fig. 5), probably due to material originating from damaged organelles and smaller parts of membranes which were not filtered out. Moreover, the protocol used does not ensure a perfect separation between the different fractions, allowing the presence of GSH and purines, to various extents, in fractions other than the cytosolic one.

Successively, SERS spectra generated by lysates of IHH cells synchronized by serum starvation were acquired (Fig. 6). Percentages of cells synchronized at 0 h and reactivated for 48 h were consistent with literature for G_0/G_1, S, and G_2/M phases (Table 1)

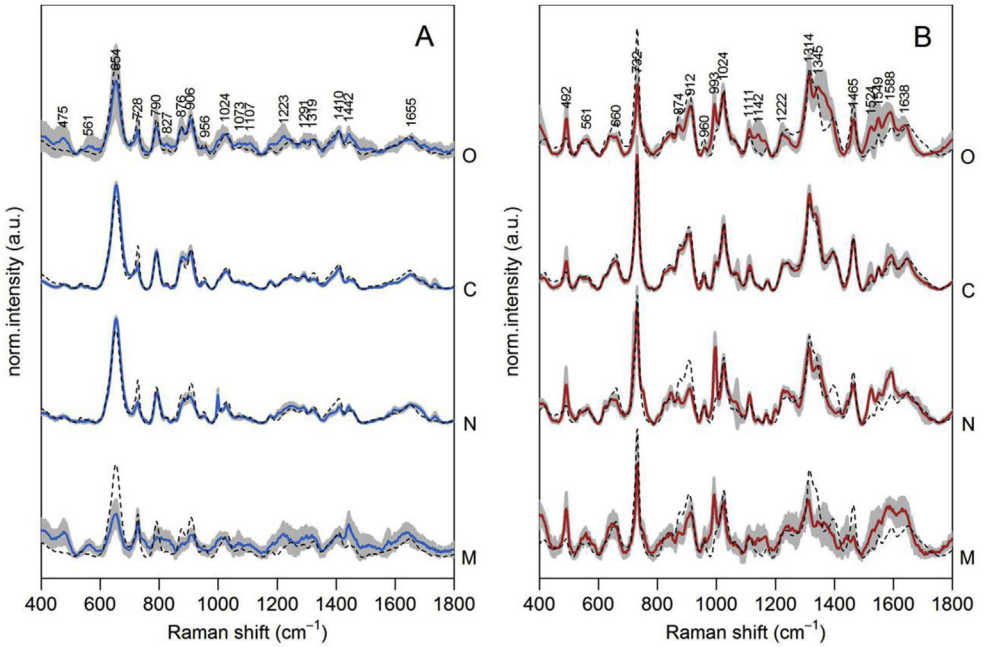

Fig. 5. Comparison between 4 different samples obtained from filtering different cell fractions separately and the overall lysate average SERS spectrum, for IHH cells lysed with sodium citrate 10 mM, for both Ag (A) and Au nanoparticles (B). Average spectra of filtered cytosol fraction (C) is shown together with those of the membranes (M), nuclei (N), and organelles (O) (intensity standard deviations are shown as shaded gray areas). Average spectra are obtained from N = 21 independent measurements out of 8 different cell cultures. The average spectrum of un-fractioned, filtered IHH lysate (same as in Fig. 1) is shown beside fraction averages for comparison (dashed black lines). All spectra were vector normalized (before averaging) for better comparison.

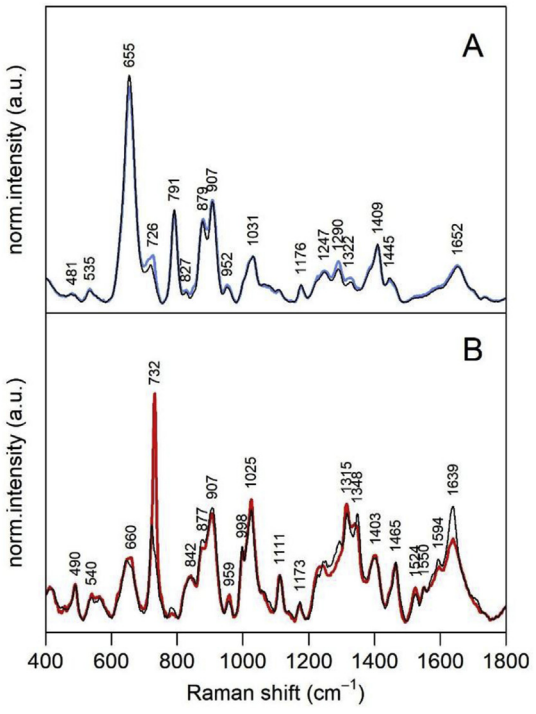

Fig. 6. Effect of starvation. Average SERS spectra of filtered lysates of starved (black lines) and reactivated (for 48 h, colored lines) IHH cells using (A) Ag and (B) Au nanoparticles as substrates. Average spectra are obtained from N = 9 independent measurements out of 3 different cell cultures. (For interpretation of the references to color in this figure legend, the reader is referred to the Web version of this article.)

[56,57]. SERS analysis with Au nanoparticles (Fig. 6B) showed that starved hepatocytes are characterized by a lower intensity of the

Table 1
Cell cycle synchronization. Percentages of IHH cells synchronized at 0 h and re-activated for 48 h.

	0 h	48 h
G_0/G_1	79.4 ± 2.4%	60.6 ± 2.5%***
S	5.7 ± 19.3%	14.0 ± 7.1%*
G_2/M	14.9 ± 6.0%	24.8 ± 14.5%**

Statistical analysis 48 h *vs* 0 h: *, p < .05; **, p < .01; ***, p < .001 (Two way ANOVA and Bonferroni's post test).

732 cm^{-1} band, due to the ring-breathing vibrational modes of adenine and adenosine, compared to those reactivated for 48 h. This effect can be due to a particular process that occurs during the cell reactivation. In fact, in the literature there are works showing that starved cells transform higher quantities of adenosine in the correspondent nucleotides ADP and ATP [58]. Moreover, a recent work demonstrates that ATP restrains cell death induced by serum deprivation [59]. In our analysis, nucleotide forms of nucleobases do not appear in SERS spectra because of the electrostatic repulsion between negatively-charged phosphate moieties and negative charges of the citrate layer on nanoparticles, as previously explained. Therefore, a likely explanation for the observed spectral changes is that, as a result of this transformation of adenine in nucleotides form during starvation, SERS spectra of starved cells display weaker adenosine/adenine bands than non-starved or re-activated cells. After starvation, hepatocytes return to physiological conditions with a consequent intensity increase of the adenosine/adenine band. This effect is more readily observed in spectra obtained using Au nanoparticles (Fig. 6B), where the bands due to purine bases are more intense. However, upon careful inspection the same phenomenon can be observed, to a lesser extent, in spectra obtained from Ag nanoparticles as well (Fig. 6A), where purines contribution to the spectrum is less pronounced.

4. Conclusions

Repeatable and stable SERS spectra of different cell lysates, which are characteristic of the cell cytosol, can be obtained using an easy and rapid pre-processing method based on filtration. The main advantage of this method with respect to studying intact cells with SERS is that the cytosol can be directly probed without the need to internalize nanoparticles into cells. The interaction between cytosolic constituents and nanoparticles, and thus the corresponding lysate SERS spectrum, is heavily influenced by the nature of metal used, with Ag favoring the observation of GSH and Au that of purine derivatives. Conversely, the type of buffer used for the lysis protocol only marginally affects the spectral structure. Differences in the SERS spectra, especially when obtained using Au substrates, allow to distinguish between different cell lines, as well as to monitor biochemical changes due to serum starvation.

References

[1] J.E. Gagner, S. Shrivastava, X. Qian, J.S. Dordick, R.W. Siegel, Engineering nanomaterials for biomedical applications requires understanding the nano-bio interface: a perspective, J. Phys. Chem. Lett. 3 (21) (2012) 3149–3158.

[2] A.E. Nel, L. Mädler, D. Velegol, T. Xia, E.M.V. Hoek, P. Somasundaran, F. Klaessig, V. Castranova, M. Thompson, Understanding biophysicochemical interactions at the nano-bio interface, Nat. Mater. 8 (7) (2009) 543–557.

[3] J. Wolfram, Y. Yang, J. Shen, A. Moten, C. Chen, H. Shen, M. Ferrari, Y. Zhao, The nano-plasma interface: implications of the protein corona, Colloids Surfaces B Biointerfaces 124 (2014) 17–24.

[4] J. Wang, W.A. Quershi, Y. Li, J. Xu, G. Nie, Analytical methods for nano-bio interface interactions, Sci. China Chem. 59 (2016) 1467–1478.

[5] X. Qian, X.-H. Peng, D.O. Ansari, Q. Yin-Goen, G.Z. Chen, D.M. Shin, L. Yang, A.N. Young, M.D. Wang, S. Nie, In vivo tumor targeting and spectroscopic detection with surface-enhanced Raman nanoparticle tags, Nat. Biotechnol. 26 (1) (2008) 83–90.

[6] M. Neshatian, C. Yang, N. Hegarty, D.B. Chithrani, Optimizing the bio-nano interface for gold nanoparticles, in: N. Baltzer, T. Copponnex (Eds.), Precious Metals for Biomedical Applications, Woodhead Publishing, Cambridge, 2014, pp. 87–106.

[7] C. Wang, L. Dong, Exploring 'new' bioactivities of polymers at the nano–bio interface, Trends Biotechnol. 33 (1) (2015) 10–14.

[8] A.M. Alkilany, S.E. Lohse, C.J. Murphy, The gold standard: gold nanoparticle libraries to understand the nano–bio interface, Acc. Chem. Res. 46 (3) (2013) 650–661.

[9] T.E. Mallouk, P. Yang, Chemistry at the nano-bio interface, J. Am. Chem. Soc. 131 (23) (2009) 7937–7939.

[10] D. Shcharbin, M. Ionov, V. Abashkin, S. Loznikova, V. Dzmitruk, N. Shcharbina, L. Matusevich, K. Milowska, K. Gałecki, S. Wysocki, M. Bryszewska, Nanoparticle corona for proteins: mechanisms of interaction between dendrimers and proteins, Colloids Surfaces B Biointerfaces 134 (2015) 377–383.

[11] A.M. Herrmann, P.L. Clode, I.R. Fletcher, N. Nunan, E.A. Stockdale, A.G. O'Donnell, D.V. Murphy, YA novel method for the study of the biophysical interface in soils using nano-scale secondary ion mass spectrometry, Rapid Commun. Mass Spectrom. RCM 21 (1) (2007) 29–34.

[12] A. Bhaumik, A.M. Shearin, R. Delong, A. Wanekaya, K. Ghosh, Probing the interaction at the nano-bio interface using Raman spectroscopy: ZnO nanoparticles and adenosine triphosphate biomolecules, J. Phys. Chem. C Nanomater. Interfaces 118 (32) (2014) 18631–18639.

[13] R. Frost, S. Svedhem, Characterization of nanoparticle-lipid membrane interactions using QCM-D, Meth. Mol. Biol. 991 (2013) 127–137.

[14] E. Smith, G. Dent, Modern Raman Spectroscopy – a Practical Approach, John Wiley & Sons, Ltd, Chichester, 2004, pp. 113–133.

[15] S. Schlücker (Ed.), Surface Enhanced Raman Spectroscopy: Analytical, Biophysical and Life Science Applications, Wiley-VCH, Weinheim, 2010.

[16] S. Schlücker, Surface-enhanced Raman spectroscopy: concepts and chemical applications, Angew. Chem. Int. Ed. 53 (19) (2014) 4756–4795.

[17] M. Moskovits, Surface-enhanced Raman spectroscopy: a brief retrospective, J. Raman Spectrosc. 36 (6–7) (2005) 485–496.

[18] M. Altunbek, G. Kuku, M. Culha, Gold nanoparticles in single-cell analysis for surface enhanced Raman scattering, Molecules 21 (12) (2016) 1617.

[19] J. Kneipp, H. Kneipp, K. Kneipp, M. McLaughlin, D. Brown, Surface-enhanced Raman scattering for investigations of eukaryotic cells, in: P. Lasch, J. Kneipp (Eds.), Biomedical Vibrational Spectroscopy, John Wiley & Sons, Inc., Hoboken, 2008, pp. 243–261.

[20] J. Kneipp, D. Drescher, SERS in cells: from concept to practical applications, in: Y. Ozaki, K. Kneipp, R. Aroca (Eds.), Frontiers of Surface-enhanced Raman Scattering, John Wiley & Sons, Ltd, Hoboken, 2014, pp. 285–308.

[21] J. Kneipp, H. Kneipp, M. McLaughlin, D. Brown, K. Kneipp, In vivo molecular probing of cellular compartments with gold nanoparticles and nanoaggregates, Nano Lett. 6 (10) (2006) 2225–2231.

[22] A. Huefner, D. Septiadi, B.D. Wilts, I.I. Patel, W.-L. Kuan, A. Fragniere, R.A. Barker, S. Mahajan, Gold nanoparticles explore cells: cellular uptake and their use as intracellular probes, Methods 68 (2) (2014) 354–363.

[23] J. Taylor, A. Huefner, L. Li, J. Wingfield, S. Mahajan, Nanoparticles and intracellular applications of surface-enhanced Raman spectroscopy, Analyst 141 (17) (2016) 5037–5055.

[24] M. Hassoun, I. W.Schie, T. Tolstik, S.E. Stanca, C. Krafft, J. Popp, Surface-enhanced Raman spectroscopy of cell lysates mixed with silver nanoparticles for tumor classification, Beilstein J. Nanotechnol. 8 (1) (2017) 1183–1190.

[25] I.J. Schippers, H. Moshage, H. Roelofsen, M. Müller, H.S. Heymans, M. Ruiters, F. Kuipers, Immortalized human hepatocytes as a tool for the study of hepatocytic (de-)differentiation, Cell Biol. Toxicol. 13 (4–5) (1997) 375–386.

[26] S. Pirkmajer, A.V. Chibalin, Serum starvation: caveat emptor, Am. J. Physiol. Cell Physiol. 301 (2) (2011) C272–C279.

[27] Z. Darzynkiewicz, H.D. Halicka, H. Zhao, Analysis of cellular DNA content by flow and laser scanning cytometry, Adv. Exp. Med. Biol. 676 (2010) 137–147.

[28] J. Kimling, M. Maier, B. Okenve, V. Kotaidis, H. Ballot, A. Plech, Turkevich method for gold nanoparticle synthesis revisited, J. Phys. Chem. B 110 (32) (2006) 15700–15707.

[29] P.C. Lee, D. Meisel, Adsorption and surface-enhanced Raman of dyes on silver and gold sols, J. Phys. Chem. 86 (1982) 3391–3395.

[30] V. Amendola, O.M. Bakr, F. Stellacci, A study of the surface plasmon resonance of silver nanoparticles by the discrete dipole approximation method: effect of shape, size, structure, and assembly, Plasmonics 5 (1) (2010) 85–97.

[31] R Core Team, R: a Language and Environment for Statistical Computing, R Foundation for Statistical Computing, Vienna, Austria, 2017. URL, https://www.R-project.org/.

[32] C. Beleites, V. Sergo, hyperSpec: a Package to Handle Hyperspectral Data Sets in R, R package version 0.98-20161118, http://hyperspec.r-forge.r-project.org.

[33] K.H. Liland, B.H. Mevik, Baseline: Baseline Correction of Spectra, 2015. R package version 1.2-1, https://CRAN.R-project.org/package=baseline.

[34] S.R. Saptarshi, A. Duschl, A.L. Lopata, Interaction of nanoparticles with proteins: relation to bio-reactivity of the nanoparticle, J. Nanobiotechnol. 11 (1) (2013) 26.

[35] V.P. Zhdanov, N.-J. Cho, Kinetics of the formation of a protein corona around nanoparticles, Math. Biosci. 282 (2016) 82–90.

[36] A. Bonifacio, S. Dalla Marta, R. Spizzo, S. Cervo, A. Steffan, A. Colombatti, V. Sergo, Surface-enhanced Raman spectroscopy of blood plasma and serum using Ag and Au nanoparticles: a systematic study, Anal. Bioanal. Chem. 406 (9–10) (2014) 2355–2365.

[37] A. Bonifacio, S. Cervo, V. Sergo, Label-free surface-enhanced Raman spectroscopy of biofluids, Anal. Bioanal. Chem. 407 (27) (2015) 8265–8277.

[38] J. Lin, R. Chen, S. Feng, Y. Li, Z. Huang, S. Xie, Y. Yu, M. Cheng, H. Zeng, Rapid delivery of silver nanoparticles into living cells by electroporation for surface-enhanced Raman spectroscopy, Biosens. Bioelectron. 25 (2) (2009) 388–394.

[39] S. Mert, M. Çulha, Surface-enhanced Raman scattering-based detection of cancerous renal cells, Appl. Spectrosc. 68 (6) (2014) 617–624.

[40] M. Pagliai, S. Caporali, M. Muniz-Miranda, G. Pratesi, V. Schettino, SERS, XPS, and DFT study of adenine adsorption on silver and gold surfaces, J. Phys. Chem. Lett. 3 (2) (2012) 242–245.

[41] J. Kundu, O. Neumann, B.G. Janesko, D. Zhang, S. Lal, A. Barhoumi, G.E. Scuseria, N.J. Halas, Adenine– and adenosine monophosphate (AMP)–Gold binding interactions studied by surface-enhanced Raman and infrared spectroscopies, J. Phys. Chem. C 113 (32) (2009) 14390–14397.

[42] B. Pergolese, A. Bonifacio, A. Bigotto, SERS studies of the adsorption of guanine derivatives on gold colloidal nanoparticles, Phys. Chem. Chem. Phys. PCCP 7 (20) (2005) 3610–3613.

[43] W.R. Premasiri, J.C. Lee, L.D. Ziegler, Surface-enhanced Raman scattering of whole human blood, blood plasma, and red blood cells: cellular processes and bioanalytical sensing, J. Phys. Chem. B 116 (31) (2012) 9376–9386.

[44] P. Hu, X.-S. Zheng, C. Zong, M.-H. Li, L.-Y. Zhang, W. Li, B. Ren, Drop-coating deposition and surface-enhanced Raman spectroscopies (DCDRS and SERS) provide complementary information of whole human tears, J. Raman Spectrosc. 45 (7) (2014) 565–573.

[45] L. Guerrini, Ž. Krpetić, D. van Lierop, R.A. Alvarez-Puebla, D. Graham, Direct surface-enhanced Raman scattering analysis of DNA duplexes, Angew. Chem. Int. Ed. 54 (4) (2015) 1144–1148.

[46] S.E.J. Bell, N.M.S. Sirimuthu, Surface-enhanced Raman spectroscopy (SERS) for sub-micromolar detection of DNA/RNA mononucleotides, J. Am. Chem. Soc. 128 (49) (2006) 15580–15581.

[47] T.W. Traut, Physiological concentrations of purines and pyrimidines, Mol. Cell. Biochem. 140 (1) (1994) 1–22.

[48] S. Gessi, S. Merighi, V. Sacchetto, C. Simioni, P.A. Borea, Adenosine receptors and cancer, Biochim. Biophys. Acta BBA - Biomembr. 1808 (5) (2011) 1400–1412.

[49] V. Kumar, Adenosine as an endogenous immunoregulator in cancer pathogenesis: where to go? Purinergic Signal. 9 (2) (2013) 145–165.

[50] Z. Peng, P.A. Borea, T. Wilder, H. Yee, L. Chiriboga, M.R. Blackburn, G. Azzena,

G. Resta, B.N. Cronstein, Adenosine signaling contributes to ethanol-induced fatty liver in mice, J. Clin. Invest. 119 (3) (2009) 582–594.
[51] R.M. Mitchell, S.Y. Lee, W.T. Randazzo, Z. Simmons, J.R. Connor, Influence of HFE variants and cellular iron on monocyte chemoattractant protein-1, J. Neuroinflammation 6 (1) (2009) 6.
[52] L. Luo, H. Uehara, X. Zhang, S.K. Das, T. Olsen, D. Holt, J.M. Simonis, K. Jackman, N. Singh, T.R. Miya, W. Huang, F. Ahmed, A. Bastos-Carvalho, Y.Z. Le, C. Mamalis, V.A. Chiodo, W.W. Hauswirth, J. Baffi, P.M. Lacal, A. Orecchia, N. Ferrara, G. Gao, K. Young-hee, Y. Fu, L. Owen, R. Albuquerque, W. Baehr, K. Thomas, D.Y. Li, K.V. Chalam, M. Shibuya, S. Grisanti, D.J. Wilson, J. Ambati, B.K. Ambati, Photoreceptor avascular privilege is shielded by soluble VEGF receptor-1, eLife 2 (2013), e00324.
[53] D. Haridass, Q. Yuan, P.D. Becker, T. Cantz, M. Iken, M. Rothe, N. Narain, M. Bock, M. Nörder, N. Legrand, H. Wedemeyer, K. Weijer, H. Spits, M.P. Manns, J. Cai, H. Deng, J.P. Di Santo, C.A. Guzman, M. Ott, Repopulation efficiencies of adult hepatocytes, fetal liver progenitor cells, and embryonic stem cell-derived hepatic cells in albumin-promoter-enhancer urokinase-type plasminogen activator mice, Am. J. Pathol. 175 (4) (2009) 1483–1492.
[54] T. Dervieux, Y. Chu, Y. Su, C.-H. Pui, W.E. Evans, M.V. Relling, HPLC determination of thiopurine nucleosides and nucleotides in vivo in lymphoblasts following mercaptopurine therapy, Clin. Chem. 48 (1) (2002) 61–68.
[55] W.C. Lim, T.W. Jordan, Subcellular distribution of hepatic bile acid-conjugating enzymes, Biochem. J. 197 (3) (1981) 611–618.
[56] R. Khammanit, S. Chantakru, Y. Kitiyanant, J. Saikhun, Effect of serum starvation and chemical inhibitors on cell cycle synchronization of canine dermal fibroblasts, Theriogenology 70 (1) (2008) 27–34.
[57] O. Hayes, B. Ramos, L.L. Rodríguez, A. Aguilar, T. Badía, F.O. Castro, Cell confluency is as efficient as serum starvation for inducing arrest in the G0/G1 phase of the cell cycle in granulosa and fibroblast cells of cattle, Anim. Reprod. Sci. 87 (3) (2005) 181–192.
[58] E. Rapaport, P.C. Zamecnik, Increased incorporation of adenosine into adenine nucleotide pools in serum-deprived mammalian cells, Proc. Natl. Acad. Sci. U. S. A. 75 (3) (1978) 1145–1147.
[59] J.L. Berlier, S. Rigutto, A. Dalla Valle, J. Lechanteur, M.S. Soyfoo, V. Gangji, J. Rasschaert, Adenosine triphosphate prevents serum deprivation-induced apoptosis in human mesenchymal stem cells via activation of the MAPK signaling pathways, Stem Cell. 33 (1) (2015) 211–218.